Diffraction theory in TM polarization: application of the fast Fourier factorization method to cylindrical devices with arbitrary cross section

Philippe Boyer, Evgeni Popov, Michel Nevière, and Gérard Tayeb

Institut Fresnel, Case 161, Unité Mixte de Recherche Associée au Centre National de la Recherche Scientifique (UMR 6133), Université d'Aix-Marseille III, Université de Provence, Faculté des Sciences et Techniques de St. Jérôme, Avenue Escadrille Normandie Niémen, 13397 Marseille Cedex 20, France

Received April 16, 2004; revised manuscript received June 22, 2004; accepted June 24, 2004

The diffraction of an electromagnetic wave by a cylindrical object with arbitrary cross section is studied by taking advantage of recent progress in grating theories. The fast Fourier factorization method previously developed in Cartesian coordinates is extended to cylindrical coordinates thanks to the periodicity of both the diffracting object and the incident wave with respect to the polar angle θ. Thus Maxwell equations in a truncated Fourier space are derived and separated in TE and TM polarization cases. The new set of equations for TM polarization is resolved numerically with the S-matrix propagation algorithm. Examples of elliptic cross sections and cross sections including couples of nonconcentric circles show fast convergence of the results, for both dielectric and metallic materials, as well as good agreement with previous published results. Thus the method is suitable for an extension to conical (out-of-plane) diffraction, which will allow studying mode propagation along microstructured fibers.

OCIS codes: 050.1960, 060.0060.

1. INTRODUCTION

Since 1960 and the advent of powerful computers, several families of diffraction theories have been developed, among which are the integral method, the modal method, the differential method, and the fictitious source method. The integral method was the first rigorous grating theory applied to perfectly conducting gratings and was quickly generalized for finite conductivity. The differential theory soon followed[1] but turned out to be limited in its application range by numerical contamination appearing in the integration process. The problem was resolved only around 20 years later by use of suitable matrix propagation algorithms,[2,3] among which the most suitable is the S-matrix propagation algorithm.[3,4] It was then possible to integrate the ordinary differential field propagation equations over thousands of wavelengths without losing significant digits. However, slow convergence of the Fourier series of the field was still seen in TM polarization. A key paper[4] pointed out that this slow convergence could result from a wrong truncation process of the Fourier series and established two factorization rules to help correct truncating. By a suitable continuation of the notion of tangential and normal components of the field in the entire modulated region, two of the authors (M. Nevière and E. Popov) applied the previous rules to obtain a new formulation of the Maxwell equations in a truncated Fourier space that has been called the fast Fourier factorization (FFF) method.[5,6]

The present paper shows the adaptation of the FFF method coupled with the S-matrix propagation algorithm in a cylindrical coordinate system. Thus we consider a cylindrical device with natural periodicity according to the angle coordinate. The TM polarization of the field is considered, since the TE case has been resolved for many years and does not require the FFF method. Several cross-section shapes are considered: elliptical cylinder, two identical circular cylinders symmetrically centered on the x axis, and one circular cylinder centered outside the origin. The numerical results are compared with the method of fictitious sources for isolated rods[7,8] and the multipole method for a finite set of parallel cylinders.[9]

2. PRESENTATION OF THE PROBLEM

We consider in Fig. 1 a cylindrical object described in both a Cartesian coordinate system $Oxyz$ and with cylindrical coordinates r, θ, z. Its surface (S) is produced by an arbitrary directrix located in the cross-section plane and generatrices that are straight lines parallel to the z axis. The equation of the directrix is $f(r, \theta) = 0$ or $r = g(\theta)$, where f and g are given functions. The surface (S) divides the space into two regions. Region 1 is contained inside the surface and is filled with a linear, homogeneous, and isotropic medium, dielectric or conductor (nonmagnetic), and its complex permittivity is denoted ϵ_1. Region 2 is the outside region with real permittivity ϵ_2. The present method requires introducing three new areas defined by two circular cylinders with directrices C_1 and C_2. The directrix C_1 is the inscribed circle to the directrix of surface (S), and C_2 is the circumscribed circle. The area included between both circular cylinders is named the modulated area; inside this area the permittivity $\epsilon(r, \theta)$ is a 2π-periodic, piecewise-constant function with respect to θ.

An incident plane wave with wave vector $\mathbf{k_2}$ contained in the cross-section plane falls on the device. We assume

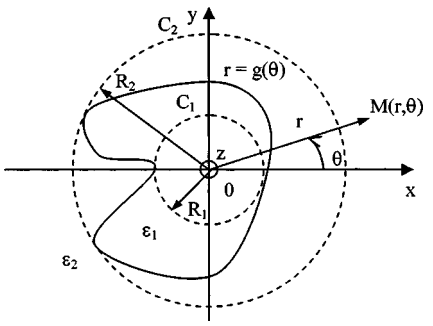

Fig. 1. Arbitrary shaped cylindrical object.

that its components have an harmonic $\exp(-i\omega t)$ time dependence. Thus the components of the incident field $\mathbf{A^{(i)}}$ read as

$$\mathbf{A^{(i)}}(r,\ \theta,\ t) = \mathbf{A_0}\exp[i(\alpha_0 r\cos\theta + \beta_0 r\sin\theta)]\exp(-i\omega t),$$
$$A \in \{E_r,\ E_\theta,\ E_z,\ H_r,\ H_\theta,\ H_z\}. \tag{1}$$

Since the diffraction problem (surface and incident wave) is z independent, the total field remains z independent. Moreover, the cylindrical coordinate system naturally implies a 2π periodicity with respect to θ. In view of a numerical implementation of the theory, any electromagnetic and geometrical quantity u will be represented by its Fourier development truncated up to the Nth order:

$$u(r,\ \theta,\ t) = \exp(-i\omega t)\sum_{n=-N}^{+N} u_n(r)\exp(in\theta),$$
$$u_n(r) = \frac{1}{2\pi}\int_0^{2\pi} u(r,\ \theta)\exp(-in\theta)\mathrm{d}\theta. \tag{2}$$

3. FAST FOURIER FACTORIZATION METHOD EXTENDED TO CYLINDRICAL COORDINATES

A. Reformulation of the Linear Relation between E and D

The first important and original point of our paper consists of adapting the FFF[6] method to cylindrical coordinates. The basic idea consists of finding the best formulation in a truncated Fourier space of a product of two discontinuous functions, each function being represented by two truncated Fourier series. This problem occurs in the modulated area when we want to calculate $\mathbf{D}$ given by

$$\mathbf{D} = \epsilon(r,\ \theta)\mathbf{E}. \tag{3}$$

In fact, the function $\epsilon(r,\ \theta)$ is discontinuous across the surface (S). The three factorization rules established by Li[4] may allow us to obtain a solution to this problem. The first rule provides that the Fourier components h_n of the product $h(x)$ of two periodic, piecewise-smooth, bounded functions $f(x)$ and $g(x)$ are given by Laurent's rule:

$$h_n = [f(x)g(x)]_n = \sum_{m=-N}^{+N} f_{n-m}g_m. \tag{4}$$

To simplify the equations that follow, we introduce the Toeplitz matrix $[\![f]\!]$ defined by $([\![f]\!])_{n,m} = f_{n-m}$ and the column vector $[g]$ with elements g_n. Thus the last equation reads in matrix notation as

$$[fg] = [\![f]\!][g]. \tag{5}$$

The second rule of Li[4] states that a product of two piecewise-smooth, bounded, periodic functions that have only pairwise-complementary jump discontinuities (i.e., that have a continuous product) cannot be factorized by Laurent's rule, but, in most cases, it can be factorized by the inverse rule:

$$[f(x)g(x)]_n = \sum_{m=-N}^{+N}\left(\left[\!\left[\frac{1}{f}\right]\!\right]^{-1}\right)_{n,m} g_m. \tag{6}$$

Or, in matrix notation,

$$[fg] = \left[\!\left[\frac{1}{f}\right]\!\right]^{-1}[g]. \tag{7}$$

Finally the most general situation concerns a product of two piecewise-smooth, bounded, periodic functions that have concurrent but not complementary jump discontinuities. Such a product can be correctly factorized neither by Laurent's rule nor by the inverse rule. This is the case that occurs in Eq. (3).

The basic idea of the FFF method is to use the first two rules to write a new formulation of Eq. (3), thanks to a suitable continuation. In the modulated area, the $\mathbf{D}$ vector is decomposed into its tangential and normal components:

$$\mathbf{D} = \epsilon(\mathbf{E}_T + \mathbf{E}_N). \tag{8}$$

The normal component of $\mathbf{D}$ is continuous across the surface (S), and the dielectric function is discontinuous. This leads to application of the inverse rule to calculate the Fourier components of $\mathbf{D}_N = \epsilon\mathbf{E}_N$. On the other hand, Laurent's rule is applied to the tangential component $\mathbf{D}_T$ of $\mathbf{D}$, since $\mathbf{E}_T$ is continuous across (S). Introducing the column vector $[\mathbf{D}]$ made by three blocks containing $2N + 1$ Fourier components of D_x, D_y, and D_z, we find that Eq. (8) becomes

$$[\mathbf{D}] = [\![\epsilon]\!][\mathbf{E}_T] + \left[\!\left[\frac{1}{\epsilon}\right]\!\right]^{-1}[\mathbf{E}_N]. \tag{9}$$

The tangential vector is derived from the normal vector by $\mathbf{E}_T = \mathbf{E} - \mathbf{E}_N$. The normal component is the scalar product between the normal vectors of the surface (S) and the field: $\mathbf{E}_N = (\mathbf{N}\cdot\mathbf{E})\mathbf{N}$. Equation (9) then reads as

$$[\mathbf{D}] = [\![\epsilon]\!][\mathbf{E}] - \left([\![\epsilon]\!] - \left[\!\left[\frac{1}{\epsilon}\right]\!\right]^{-1}\right)[(\mathbf{N}\cdot\mathbf{E})\mathbf{N}]. \tag{10}$$

Besides, we define the matrix noted $(\mathbf{NN})$ by $(\mathbf{NN})_{ij} = N_iN_j$ with $i, j = r,\ \theta, z$. Since the surface is z independent, $N_z = 0$. Finally, we obtain

$$[\mathbf{D}] = Q_\epsilon(r)[\mathbf{E}], \tag{11}$$

with

$$Q_\epsilon(r) = \begin{bmatrix} [\![\epsilon]\!][\![N_\theta^2]\!] + \left[\!\left[\frac{1}{\epsilon}\right]\!\right]^{-1}[\![N_r^2]\!] & -\left([\![\epsilon]\!] - \left[\!\left[\frac{1}{\epsilon}\right]\!\right]^{-1}\right)[\![N_r N_\theta]\!] & 0 \\ -\left([\![\epsilon]\!] - \left[\!\left[\frac{1}{\epsilon}\right]\!\right]^{-1}\right)[\![N_r N_\theta]\!] & [\![\epsilon]\!][\![N_r^2]\!] + \left[\!\left[\frac{1}{\epsilon}\right]\!\right]^{-1}[\![N_\theta^2]\!] & 0 \\ 0 & 0 & [\![\epsilon]\!] \end{bmatrix}. \quad (12)$$

The size of this matrix is $3(2N+1) \times 3(2N+1)$. Moreover, we notice that the matrix Q_ϵ contains the Toeplitz matrices $[\![N_r^2]\!]$, $[\![N_\theta^2]\!]$, and $[\![N_r N_\theta]\!]$. But N_r and N_θ are defined only on the surface (S); that is why we need to extend their definition inside the whole modulated area. The extension is done in the following way. The unit vector normal to the surface (S) reads as

$$\mathbf{N}(r = g(\theta),\ \theta) = \left(\frac{\mathbf{grad}(f)}{|\mathbf{grad}(f)|}\right)_{r=g(\theta)},$$

$$f(r,\ \theta) = r - g(\theta) = 0. \quad (13)$$

From its definition, $\mathbf{N}$ depends only on θ and is defined on S only. But we extend its definition in the entire modulated area ($R_1 < r < R_2$) by introducing a new vector continuous across the diffracting surface S and defined by

$$\forall r \in [R_1,\ R_2], \qquad \mathbf{N}(r,\ \theta) = \frac{\mathbf{grad}(f)}{|\mathbf{grad}(f)|}. \quad (14)$$

We could use another method that would lead to similar numerical results.

B. Maxwell Equations in a Truncated Fourier Space—the TM Case

Differentiating the series in Eq. (2) with respect to θ results in multiplying the nth term by in. Thus, introducing a diagonal matrix α such as $(\alpha)_{nm} = n\,\delta_{nm}$, we find that the derivation reads in matrix notation as

$$\partial[A]/\partial\theta = i\alpha[A]. \quad (15)$$

Consequently, Maxwell equations written in a cylindrical coordinate system become

$$\frac{1}{r}\alpha[E_z] = \omega\mu_0[H_r], \quad (16)$$

$$\frac{\mathrm{d}[E_z]}{\mathrm{d}r} = -i\omega\mu_0[H_\theta], \quad (17)$$

$$\frac{1}{r}\left([E_\theta] + r\frac{\mathrm{d}[E_\theta]}{\mathrm{d}r} - i\alpha[E_r]\right) = i\omega\mu_0[H_z], \quad (18)$$

$$\frac{1}{r}\alpha[H_z] = -\omega[D_r], \quad (19)$$

$$\frac{\mathrm{d}[H_z]}{\mathrm{d}r} = i\omega[D_\theta], \quad (20)$$

$$\frac{1}{r}\left([H_\theta] + r\frac{\mathrm{d}[H_\theta]}{\mathrm{d}r} - i\alpha[H_r]\right) = -i\omega[D_z]. \quad (21)$$

From Eq. (11) we obtain the expression of each component of [**D**] in a cylindrical coordinate system in terms of the **E** components. We then notice that Eqs. (16)–(21) are split into two independent differential sets. The first one, including Eqs. (16), (17), and (21), is the TE polarization case with unknown functions E_z and H_θ; the other one corresponding to E_θ and H_z components is the TM case. The first one is well known and has been resolved for a long time because it does not need the FFF method or, more precisely, the second factorization rule. That is why we concentrate on the TM case corresponding to Eqs. (18), (19), and (20). With the use of the following notation,

$$Q_\epsilon = \begin{bmatrix} Q_{\epsilon,rr} & Q_{\epsilon,r\theta} & 0 \\ Q_{\epsilon,\theta r} & Q_{\epsilon,\theta\theta} & 0 \\ 0 & 0 & Q_{\epsilon,zz} \end{bmatrix}, \quad (22)$$

Eq. (20) reads as

$$\frac{\mathrm{d}[H_z]}{\mathrm{d}r} = i\omega Q_{\epsilon,\theta r}[E_r] + i\omega Q_{\epsilon,\theta\theta}[E_\theta]. \quad (23)$$

And Eq. (19) becomes

$$[E_r] = -\frac{1}{r\omega}Q_{\epsilon,rr}^{-1}\alpha[H_z] - Q_{\epsilon,rr}^{-1}Q_{\epsilon,r\theta}[E_\theta]. \quad (24)$$

These two last equations permit us to obtain

$$\frac{\mathrm{d}[H_z]}{\mathrm{d}r} = i\omega(Q_{\epsilon,\theta\theta} - Q_{\epsilon,\theta r}Q_{\epsilon,rr}^{-1}Q_{\epsilon,r\theta})[E_\theta] - \frac{i}{r}Q_{\epsilon,\theta r}Q_{\epsilon,rr}^{-1}\alpha[H_z]. \quad (25)$$

In the same way, we deduce from Eqs. (18) and (24)

$$\frac{\mathrm{d}[E_\theta]}{\mathrm{d}r} = -\frac{1}{r}(i\alpha Q_{\epsilon,rr}^{-1}Q_{\epsilon,r\theta} + I_d)[E_\theta] + i\left(\omega\mu_0 I_d - \frac{1}{r^2\omega}\alpha Q_{\epsilon,rr}^{-1}\alpha\right)[H_z], \quad (26)$$

where I_d is the identity matrix. Finally, we obtain a set of first-order differential equations written in matrix form:

$$\frac{\mathrm{d}}{\mathrm{d}r}\begin{pmatrix}[E_\theta] \\ [H_z]\end{pmatrix} = \begin{bmatrix} M_{11} & M_{12} \\ M_{21} & M_{22}\end{bmatrix}\begin{pmatrix}[E_\theta] \\ [H_z]\end{pmatrix}. \quad (27)$$

It is important to notice that the four-block matrix M is depending only on the r coordinate and that its size is $2(2N+1) \times 2(2N+1)$. Equation (27) is the new formulation of Maxwell equations in a truncated Fourier space for the TM case of polarization.

4. RESOLUTION OF THE DIFFRACTION PROBLEM

A. Field Expressions in the Homogeneous Regions

According to the r dependence of the M matrix, no explicit expression of the field in the modulated area can be found. On the other hand, Maxwell equations in the homogeneous regions ($j = 1$ or 2) permit us to obtain a set of independent second-order differential equations for the z component of the magnetic field:

$$(k_j r)^2 \frac{\mathrm{d}^2 H_{z,n}}{\mathrm{d}z^2} + k_j r \frac{\mathrm{d}H_{z,n}}{\mathrm{d}z} + [(k_j r)^2 - n^2] H_{z,n} = 0. \tag{28}$$

These equations have explicit solutions given by

$$H_{z,n} = A_{h,n}^{(j)} J_n(k_j r) + B_{h,n}^{(j)} H_n^{(j)}(k_j r), \tag{29}$$

with $k_j^2 = \omega^2 \mu_0 \epsilon_j$ and $\mathrm{Re}(k_j) + \mathrm{Im}(k_j) \geqslant 0$. The other components of the field are derived from Maxwell equations written in a homogeneous region:

$$E_r = \frac{i}{\epsilon \omega r} \frac{\partial H_z}{\partial \theta},$$

$$E_\theta = -\frac{i}{\epsilon \omega} \frac{\partial H_z}{\partial r},$$

$$H_r = -\frac{i}{\mu_0 \omega r} \frac{\partial E_z}{\partial \theta},$$

$$H_\theta = \frac{i}{\mu_0 \omega} \frac{\partial E_z}{\partial r}. \tag{30}$$

Equations (29) and (30), which allow us to find the components of the development of the fields, can be written in a matrix form. Thus we define matrix $\Psi^{(j)}$, which links the vector $[F(R_j)]$ containing the components of successive E_θ and H_z with the vector $[V^{(j)}]$ containing the components $A_{h,n}^{(j)}$ and $B_{h,n}^{(j)}$, by

$$[F(R_j)] = \begin{bmatrix} \psi_{11}^{(j)} & \psi_{12}^{(j)} \\ \psi_{21}^{(j)} & \psi_{22}^{(j)} \end{bmatrix} [V^{(j)}], \tag{31}$$

with

$$(\Psi_{11})_{nm} = -\frac{i}{\omega \epsilon_j} \left[\frac{n}{R_j} J_n(k_j R_j) - k_j J_{n+1}(k_j R_j) \right] \delta_{nm},$$

$$(\Psi_{12})_{nm} = -\frac{i}{\omega \epsilon_j} \left[\frac{n}{R_j} H_n^+(k_j R_j) - k_j H_{n+1}^+(k_j R_j) \right] \delta_{nm},$$

$$(\Psi_{21})_{nm} = J_n(k_j R_j) \delta_{nm},$$

$$(\Psi_{22})_{nm} = H_n^+(k_j R_j) \delta_{nm}.$$

We notice that the size of vectors $[F(R_j)]$ and $[V^{(j)}]$ is $2(2N + 1)$.

B. Integration of the Differential Set

The algorithm that integrates the set (27) uses a shooting method that consists of changing the boundary-value problem into an initial-value problem. In fact, we have the continuity of the tangential components of the field across circles C_1 and C_2 with radius R_1 and R_2. That is why we have chosen the z and θ components of the field as unknown functions of the differential set (27). We take $2(2N + 1)$ independent initial vectors denoted $\hat{V}_p$:

$$(\hat{V}_p)_i = \delta_{pi}, \qquad i \in [1, 2(2N + 1)]. \tag{32}$$

Putting these vectors into columns, we form the unit matrix $[\hat{V}_1] = (\ldots, \hat{V}_p, \ldots) = I_d$, and the corresponding fields read as $[F(R_1)] = \Psi^{(1)} I_d = \Psi^{(1)}$ at $r = R_1$. We use that value of $[F(R_1)]$ as initial values of the field introduced into the algorithm, which integrates the differential system. The result is a matrix denoted $[\hat{F}_{\mathrm{int}}(R_2)]$ that gives the field at R_2, and the components $A_{h,n}^{(2)}$ and $B_{h,n}^{(2)}$ are deduced by $[\hat{V}_2] = \Psi^{(2)-1}[\hat{F}_{\mathrm{int}}(R_2)]$; since $[\hat{V}_1] = I_d$, we obtain $[\hat{V}_2] = \Psi^{(2)-1}[\hat{F}_{\mathrm{int}}(R_2)][\hat{V}_1]$. Recalling that the operator that links the components at R_1 and R_2 is the transmission or T matrix, we simply obtain

$$T = \Psi^{(2)-1}[\hat{F}_{\mathrm{int}}(R_2)]. \tag{33}$$

The T matrix depends only on the system (S). Thus it gives the transmitted field corresponding to any incident wave. In fact, according to the following Bessel development, Eq. (1) can be written as

$$H_z^{(i)} = \sum_{n=-\infty}^{+\infty} A_{h,z} \exp(-in\theta_i) i^n J_n(k_2 r) \exp(in\theta), \tag{34}$$

where θ_i is the angle between the wave vector of the incident field and the x axis and $A_{h,z}$ is the amplitude of the incident wave. Finally, introducing the T_{ij} blocks of the T matrix, we obtain

$$\begin{pmatrix} \vdots \\ A_{h,n}^{(1)} \\ \vdots \end{pmatrix} = T_{11}^{-1} \begin{pmatrix} \vdots \\ A_{h,z} i^n \exp(-in\theta_i) \\ \vdots \end{pmatrix}, \tag{35}$$

$$\begin{pmatrix} \vdots \\ B_{h,n}^{(2)} \\ \vdots \end{pmatrix} = T_{21} T_{11}^{-1} \begin{pmatrix} \vdots \\ A_{h,z} i^n \exp(-in\theta_i) \\ \vdots \end{pmatrix}. \tag{36}$$

5. NUMERICAL APPLICATION IN SOME PARTICULAR CASES

A. Cylinder with Elliptic Cross Section

First of all, we illustrate our study on a diffracting surface directrix with elliptic shape (Fig. 2) given by

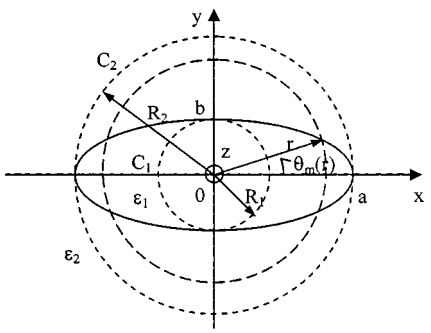

Fig. 2. Elliptically shaped cylindrical object.

$$r(\theta) = \frac{ab}{[a^2 + (b^2 - a^2)\cos^2\theta]^{1/2}}, \tag{37}$$

where a and b are the half-large and the small axis, respectively. Then the calculus of the permittivity's development becomes easy, since the permittivity is a step function with respect to θ. On the other hand, the functions that describe the θ and r components of the surface's normal vector remain difficult to Fourier analyze. Their equations are

$$N_r(\theta) = \frac{a^2 + (b^2 - a^2)\cos^2\theta}{\{[a^2 + (b^2 - a^2)\cos^2\theta]^2 + (a^2 - b^2)^2\sin^2\theta\cos^2\theta\}^{1/2}}, \tag{38}$$

$$N_\theta(\theta) = \frac{(a^2 - b^2)\sin\theta\cos\theta}{\{[a^2 + (b^2 - a^2)\cos^2\theta]^2 + (a^2 - b^2)^2\sin^2\theta\cos^2\theta\}^{1/2}}. \tag{39}$$

Thus we have used the fast Fourier transformation algorithm to determine the Fourier components of these functions. As a result, the Toeplitz matrices $[\![\epsilon]\!]$, $[\![N_r^2]\!]$, and $[\![N_\theta^2]\!]$ are known.

At infinity the diffracted field can be expressed by using the asymptotic form of the Hankel functions:

$$H_z^d(r, \theta, t) = \exp(-i\omega t)g(\theta)\frac{\exp(ik_2 r)}{\sqrt{r}},$$

$$g(\theta) = \left(\frac{2}{\pi k_2}\right)^{1/2}\sum_{n=-\infty}^{+\infty} B_{h,n}^{(2)} \times \exp\left[in\left(\theta - \frac{\pi}{2}\right)\right]. \tag{40}$$

The corresponding intensity called the differential cross section is defined by

$$D(\theta) = 2\pi|g(\theta)|^2. \tag{41}$$

To validate results, we compare the differential cross section calculated with the present (FFF) method and the one determined with another method (fictitious source method). In addition, our theory reduces to the classical differential method if $[\![N_r^2]\!] = \mathrm{I}$ and $[\![N_\theta^2]\!] = [\![N_r N_\theta]\!] = 0$. The comparison with the classical differential method points out the improvement due to the FFF method concerning the convergence of the differential cross-section function for a given θ when the N order is increased.

The T-matrix propagation algorithm has been applied to a device filled with a dielectric medium. Thus the index is a real number, and we choose $n_1 = 5$. The outside region is the vacuum ($n_2 = 1$). Such a index gap is chosen to stress the improvement due to the FFF method. In fact, we need more components to described the piecewise-constant function of the permittivity in the modulated area than for a conventional dielectric. The incident wave vector is parallel to the x axis ($\theta_i = 0$), and the wavelengh is $\lambda = 1$. We notice that it is not necessary to specify the unity of lengths because it can be normalized to the device dimension. According to the device parameters, we take a modulation of 50%, which means $a = 1.5$ and $b = 1$. Figure 3 shows the convergence of $D(0)$ (transmitted diffracted field) when N is increased. We notice that the convergence obtained with the FFF method is faster than the one obtained with the classical differential theory, which becomes clear when $N \geqslant 35$. Moreover, the relative discrepancy between the FFF method values and the fictitious source method ones are below 1% as soon as $N \geqslant 46$. Figure 4 shows the differential cross-section graph with the fictitious source method and with the FFF method for $N = 50$. The average relative discrepancy is approximately 2.5% for points such as values over unity. The cross-section field map (Fig. 5) shows that an important index gap implies important fluctuations of the field in the elliptical cross-section cylinder; that is why several development components are needed ($N > 50$).

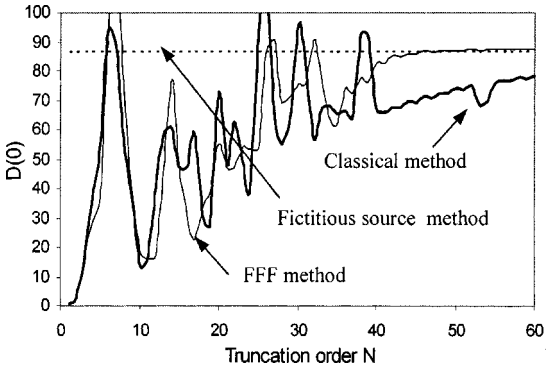

Fig. 3. Convergence of a differential cross section evaluated to 0° according to truncation order.

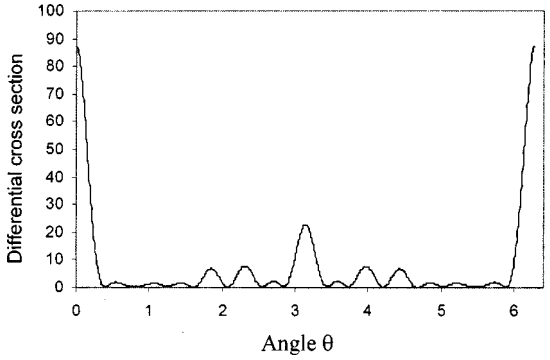

Fig. 4. Differential cross section according to the angle coordinate $D(\theta)$.

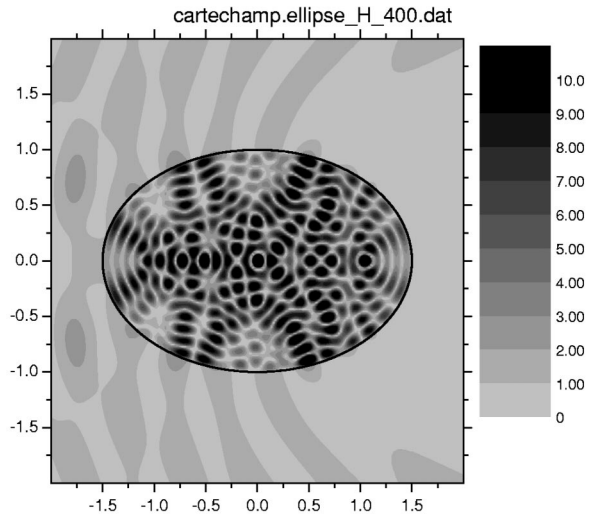

Fig. 5. Cross-section field map.

B. Numerical Contamination and *S*-Matrix Propagation Algorithm

The *T*-matrix propagation algorithm has a limitation owing to the loss of digits during the numerical integration. In fact, this algorithm does not work well when it is applied to devices with deep modulated areas and low permittivity values. The arguments of the used Hankel functions H_n^+ are $k_j r$. But these functions become singular when $r \to 0$. Moreover, the higher the n subscripts are, the higher the functions' values are, for a constant argument. Thus, when the N order is high, a loss of digits may appear, since the functions' values exceed the number memory size (16 bits). The occurrence of unbounded blocks of the T matrix implies that this loss of digits can increase during the integration process. That is why an important depth of the modulated area produces numerical contamination. For instance, when the modulation is 200% ($b = 1$ and $a = 3$), with $n_1 = 2\,(n_2 = 1)$, the divergence of $D(0)$ occurs as soon as $N = 38$. However, when $n_1 = 5$, the divergence occurs for $N \geqslant 41$.

To improve the convergence of the results, the *S*-matrix propagation algorithm is used. The modulated area is divided into M slices. The integration through each slice provides a T matrix from which we deduce a S matrix defined by

$$\forall j \in [2, M], \qquad \begin{pmatrix} \vdots \\ B_{h,n}^{(j)} \\ \vdots \\ A_{h,n}^{(1)} \\ \vdots \end{pmatrix} = \begin{pmatrix} S_{11}^{(j)} & S_{12}^{(j)} \\ S_{21}^{(j)} & S_{22}^{(j)} \end{pmatrix} \begin{pmatrix} \vdots \\ B_{h,n}^{(1)} \\ \vdots \\ A_{h,n}^{(j)} \\ \vdots \end{pmatrix}. \tag{42}$$

All blocks of this matrix are well conditioned. Briefly, the T matrix links the fields in medium (1) and the fields in medium (2), and the S matrix links the scattered field and the incident field. The *S*-matrix blocks of the jth slice are expressed according to $(j-1)$th slice's ones and the *T*-matrix blocks of the jth slice:

$$\begin{aligned} S_{22}^{(j)} &= S_{22}^{(j-1)}[T_{11}^{(j)} + T_{12}^{(j)} S_{12}^{(j-1)}]^{-1}, \\ S_{12}^{(j)} &= [T_{21}^{(j)} + T_{22}^{(j)} S_{12}^{(j-1)}][T_{11}^{(j)} \\ &\quad + T_{12}^{(j)} S_{12}^{(j-1)}]^{-1}. \end{aligned} \tag{43}$$

At the end of the integration across the modulated area, we obtain the S matrix of the whole scattered device. Thus the diffracted fields read as

$$\begin{aligned} \begin{pmatrix} \vdots \\ A_{h,n}^{(1)} \\ \vdots \end{pmatrix} &= S_{22} \begin{pmatrix} \vdots \\ A_{h,z} i^n \exp(-in\theta_i) \\ \vdots \end{pmatrix}, \\ \begin{pmatrix} \vdots \\ B_{h,n}^{(2)} \\ \vdots \end{pmatrix} &= S_{12} \begin{pmatrix} \vdots \\ A_{h,z} i^n \exp(-in\theta_i) \\ \vdots \end{pmatrix}. \end{aligned} \tag{44}$$

We expect that dealing with a complex permittivity would increase the numerical contamination. This is a guess based on our experience in grating theories that use the FFF method in a Cartesian coordinate system.[6] In this coordinate system, the fields are expressed by Fourier–Rayleigh developments. A complex permittivity implies that the field developments contain exponential functions linked with evanescent waves. Thus high arguments lead to high function values and worsen the contamination problems. To be precise, in a cylindrical coordinate system, numerical contamination occurs with an elliptic cross-section cylinder filled with aluminum ($n_1 = 1.3 + i7.6$) for $\lambda = 0.63$ and, for example, when $a = 1.5$ and $b = 1\,(\theta_i = 0)$. When the *S*-matrix propagation algorithm is applied with M equal to 10, we obtain a good convergence with respect to N. The convergence test illustrated in Fig. 6 shows a more important differ-

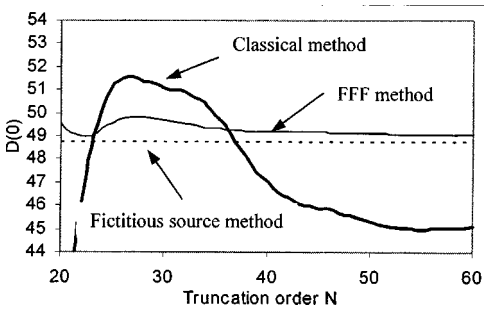

Fig. 6. Convergence of a differential cross section evaluated to 0° according to truncation order.

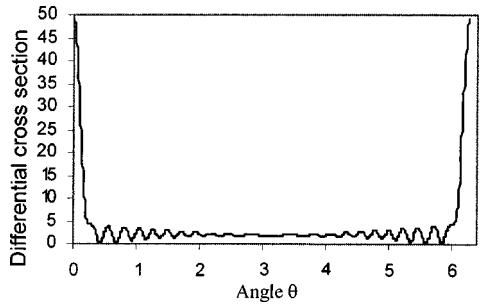

Fig. 7. Differential cross section according to the angle coordinate $D(\theta)$.

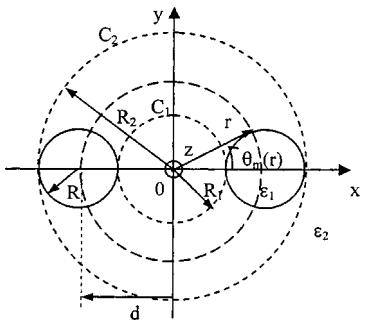

Fig. 8. Device made of two identical circular cylinders.

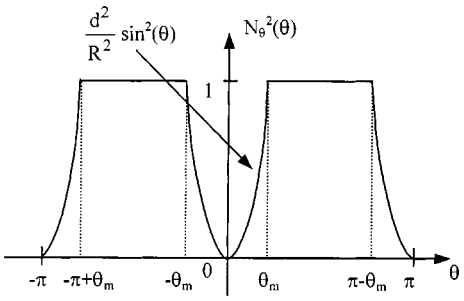

Fig. 9. First extension of N_θ^2.

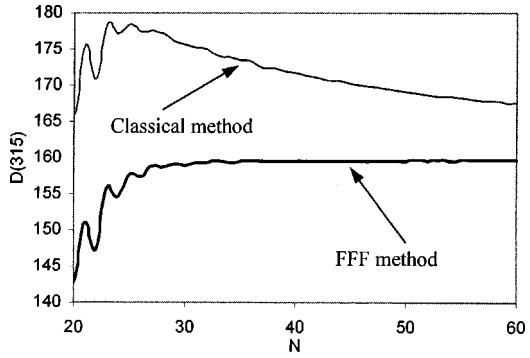

Fig. 10. Convergence of a differential cross section evaluated to 315° according to truncation order.

ence between the two methods for high orders than in the previous test. The corresponding differential cross-section graph for $N = 40$ is shown in Fig. 7.

C. Study on Other Cross-Section Shapes

From now on, we always use the S matrix propagation algorithm. We extend the study to other cross-section shapes. The first device is made of two identical circular cylinders symmetrically centered on the x axis (Fig. 8). The distance between the two centers is denoted $2d$, and their radius is R. Moreover θ_m is the maximal polar angle of a point on the circle centered at $x = d$, and the corresponding radius is r_m. It is interesting to notice that the continuation of N_θ^2 (N_r^2 and $N_r N_\theta$) is different from the previous one. We cannot use Eq. (14) for $\theta = 0$ to 2π; that is why we choose to apply two new different continuations.

First, the circle is divided in two integration layers: The first one lies between $d - R$ and r_m, and the second one lies between r_m and $d + R$. In fact, the product $N_r N_\theta$ changes its sign across the circle with radius r_m. In one of the two layers, N_θ^2 is extended with Eq. (14) for $\theta \in [-\pi, -\pi + \theta_m] \cup [-\theta_m, \theta_m] \cup [\pi - \theta_m, \pi]$. Elsewhere, N_θ^2 is extended to unity. This is illustrated in Fig. 9. This first extension is not r dependent. Consequently, the N_θ^2, N_r^2, and $N_r N_\theta$ Toeplitz matrices are calculated only once before the numerical integration, which results in saving computation time. Figures 10 and 11 show the results for $d = 4.5$, $R = 3$, $n_1 = 1.5$, $n_2 = 1$, and $\theta_i = -45°$.

The second extension is r and θ dependent, but the N_θ^2 function increases more gently. In fact, the modulation area is divided in three integration layers. N_θ^2 is defined only on four points. Elsewhere, the extension is made of

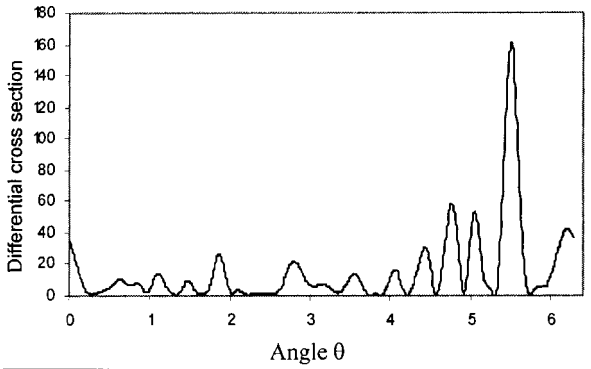

Fig. 11. Differential cross section according to angle coordinate $D(\theta)$.

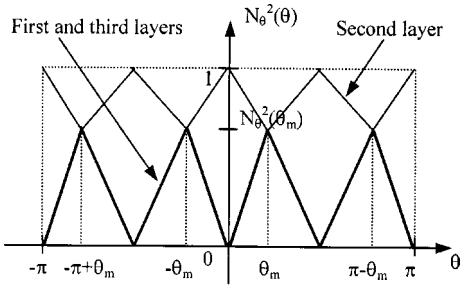

Fig. 12. Second extension of N_θ^2.

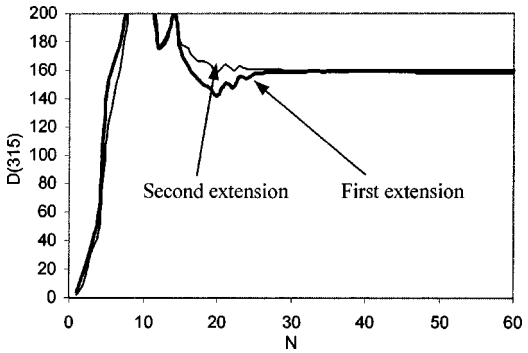

Fig. 13. Convergence of a differential cross section evaluated to 315° according to truncation order.

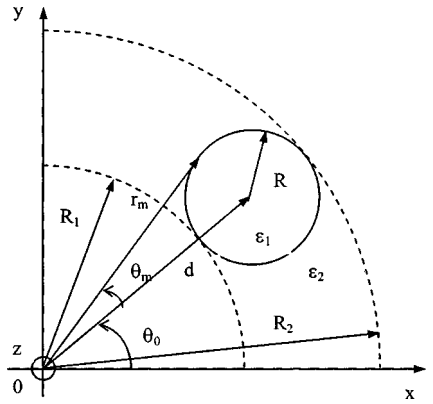

Fig. 14. Device made of one circular cylinder.

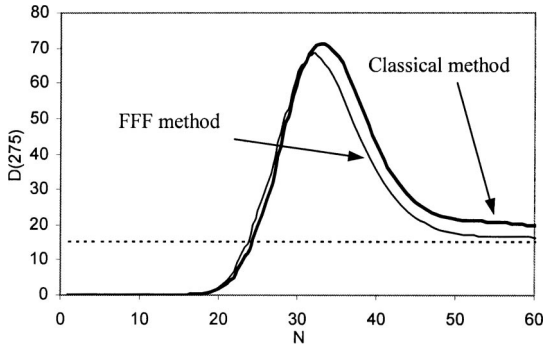

Fig. 15. Convergence of a differential cross section evaluated to 275° according to truncation order.

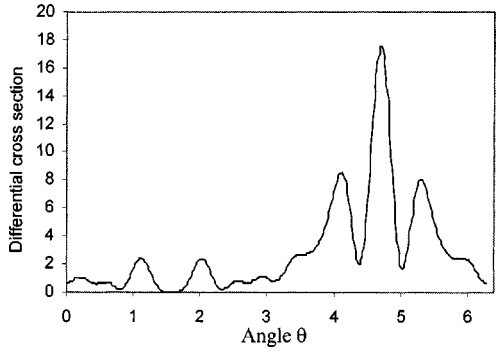

Fig. 16. Differential cross section according to angle coordinate $D(\theta)$.

straight lines. The N_θ^2 functions for the various layers are illustrated in Fig. 12. We expect that the convergence with respect to N with this second extension will be a little faster than with the first one. This is confirmed in Fig. 13.

The last studied device is simply a circle with radius R and center with (d, θ_0) polar coordinates (see Fig. 14). The maximal angle (in relation with θ_0) defined on the circle is still denoted θ_m. The chosen continuation is the same as the first one used for the previous device. The convergence test with respect to N (Fig. 15) is shown for a cylinder with $n_1 = 1.5\,(n_2 = 1)$, $d = 4$, $\theta_0 = 0°$, $R = 1$ and $\theta_i = -90°\,(\lambda = 1)$. We have verified that the differential cross-section (Fig. 16) graph remains unchanged when the circle location changes.

6. CONCLUSION

The fast Fourier factorization method, which was developed for solving diffraction of light by periodic devices such as gratings, has been extended to apparently nonperiodic devices such as cylinders, thanks to the fact that these objects are indeed periodic with respect to the angular (θ) coordinate. The fast convergence of the method has been shown on various examples.

Although the existence of numerical contamination was not evident, since in the present problem no evanescent order exists, the use of the S-matrix propagation algorithm has turned out to be necessary. This comes from the growing of some Bessel functions with complex arguments, during the integration process. Combining both methods has resulted in a theory capable of analyzing diffracting objects described in cylindrical coordinates with the same success as was previously done for periodic devices described in Cartesian coordinates.

The next stage of this work will be to generalize these equations to the conical diffraction case that implies an important increase of the matrix sizes and, consequently, of the computing time. This future study would permit one to determine the propagation modes for new microstructured optical fibers.

The successful extension of the FFF method to cylindrical coordinate provides hope of extending it to spherical coordinates, in view of deriving a theory able to analyze any three-dimensional arbitrary object.

REFERENCES

1. R. Petit, *Electromagnetic Theory of Grating* (Springer-Verlag, Berlin, 1980).
2. F. Montiel and M. Nevière, "Differential theory of gratings: extension to deep gratings of arbitrary profile and permittivity through the R-matrix propagation algorithm," J. Opt. Soc. Am. A **11**, 3241–3250 (1994).
3. L. Li, "Formulation and comparison of two recursive matrix algorithms for modeling layered diffraction gratings," J. Opt. Soc. Am. A **13**, 1024–1035 (1996).
4. L. Li, "Use of Fourier series in the analysis of discontinuous periodic structures," J. Opt. Soc. Am. A **13**, 1870–1876 (1996).
5. E. Popov and M. Nevière, "Maxwell equations in Fourier space: fast converging formulation for diffraction by arbitrary shaped, periodic, anisotropic media," J. Opt. Soc. Am. A **18**, 2886–2894 (2001).
6. M. Nevière and E. Popov, *Light Propagation in Periodic Media: Differential Theory and Design* (Marcel Dekker, New York, 2003).
7. G. Tayeb, "The method of fictitious sources applied to diffraction gratings," special issue on Generalized Multipole Techniques (GMT), Appl. Comput. Electromagn. Soc. J. **9**, 90–100 (1994).
8. F. Zolla, R. Petit, and M. Cadilhac, "Electromagnetic theory of diffraction by a system of parallel rods: the method of fictitious sources," J. Opt. Soc. Am. A **11**, 1087–1096 (1994).
9. D. Felbacq, G. Tayeb, and D. Maystre, "Scattering by a random set of parallel cylinders," J. Opt. Soc. Am. A **11**, 2526–2538 (1994).